Romanian Reports in Physics **74**, 405 (2022)

VALLEY HALL EDGE SOLITONS IN THE KAGOME PHOTONIC LATTICE

QIAN TANG[1], BOQUAN REN[2], MILIVOJ R. BELIĆ[3], YIQI ZHANG[2,*], YONGDONG LI[2]

[1]Ministry of Education Key Laboratory for Nonequilibrium Synthesis and Modulation of Condensed Matter, Shaanxi Province Key Laboratory of Quantum Information and Quantum Optoelectronic Devices, School of Physics, Xi'an Jiaotong University, Xi'an 710049, China
[2]Key Laboratory for Physical Electronics and Devices of the Ministry of Education & Shaanxi Key Lab. of Information Photonic Technique, School of Electronic Science and Engineering, Xi'an Jiaotong University, Xi'an 710049, China
[3]Science Program, Texas A&M University at Qatar, P. O. Box 23874 Doha, Qatar
[*]*zhangyiqi@xjtu.edu.cn*

Received February 12, 2022

Abstract. After more than 10 years in development, the nonlinear topological photonics is emerging as a new branch of physics. One of the most interesting subjects in the nonlinear topological photonics are the topological edge solitons. These solitary structures move along the edges of photonic crystals with constant speed, are immune to disorders/defects along the way, and maintain their profiles unchanged during long-distance propagation. In this paper, we present bright and dark valley Hall edge solitons in the kagome photonic lattice. These solitons emerge at domain walls that exist between different types of kagome lattices. We are interested in the wall between two specific types: the squeezed and expanded kagome photonic lattices. The solitons move along the wall without change in their profiles, thanks to the self-action effect of nonlinearity, and can circumvent sharp corners, thanks to the topological protection. Advances achieved in this paper represent new progress in the nonlinear topological photonics and may lead to applications in the development of novel photonic chips.

Key words: kagome lattices, valley Hall edge solitons, topological protection.

1. INTRODUCTION

The topological insulator is a new phase of matter that originated in the condensed matter physics [1, 2]. Along the rapid developement in the 21st century, it brought intriguing new phenomena to the attention of researchers in other fields of physics. It is already accepted that topological insulators may even bring improvements in the performance of electronic chips. They possess localized states that can uniformly move along the edges of photonic crystals and are immune to disorders or defects along the way. Nowadays, research on topological insulators has spread into many branches of physics, such as photonics [3–12], acoustics [13–18], mechanical systems [19, 20], ultra-cold atoms [21, 22], polaritons in microcavities [23–25], and electrical circuits [26–31]. Especially, "topological photonics" has become a completely new academic discipline that developed rapidly in the past decade [32–41],

and has already sprouted several branches, such as nonlinear topological photonics [35], non-Hermitian topological photonics [39, 42], and quantum topological photonics [43]. The present status of work on the optical topological edge solitons that belong to the nonlinear topological photonics, indeed elucidates a variety of possible avenues in the manipulation of topological edge states: bistability effects for edge states in pumped dissipative systems [44–46], modulational instability of the nonlinear edge states [47, 48], the stabilization of operation of topological lasers due to nonlinear gain saturation [49–57], nonlinearity-induced topological transitions [11], as well as a rich variety of solitonic effects [58–60], including the formation of self-sustained localized states in the bulk of topological insulators [10, 61], nonlinear vortices [62], topological edge solitons [63–76], defect solitons [77, 78], and nonlinearity-induced higher-order topological phases [79], to name a few.

Among topological edge solitons, the valley Hall edge solitons acquired special status. The term valley Hall comes from the focus on the Hall effect at the peaks and valleys in the energy band structure of photonic crystals. Such solitons do not require either external magnetic field or elaborate waveguide arrays, and therefore possess advantages in experimental realization, which is why we chose them initially for theoretical exploration. In the previous work, the valley Hall effect [80] was obtained *via* breaking the inversion symmetry of the system by introducing a detuning to the refractive index change of the waveguide channel or by adjusting the size of the lattice sites. However, such a scheme is not feasible for the kagome photonic lattice, which has three sites in the unit cell, and exhibit Dirac points as well as flat bands in the band structure [72, 81–83]. Therefore, one has to manipulate the kagome lattice differently. This is accomplished by introducing two types of misalignments in the unit cell that is adopted for the production of higher-order topological insulators [84–90], and then establishing a domain wall between the two misaligned lattices. This we achieved by squeezing sites in the unit cell in one part of the lattice and expanding them in the other, and then producing a domain wall between the squeezed and expanded sublattices that allows for the generation and propagation of valley Hall edge solitons .

Explicitly, such an operation does not break the inversion symmetry of the lattice, but indeed leads to the disappearance of Dirac points and the formation of six valleys. The Berry curvature of the valley is not zero any longer, and the sign of the Berry curvature of neighboring valleys is opposite [91, 92]. As a result, across the domain wall or the interface between squeezed and expanded kagome photonic lattices, the difference of the valley Chern numbers is ± 1, which illustrates that there is an edge state localized at the domain wall, according to the bulk-edge correspondence principle [46]. Even though valley Hall edge solitons have been reported previously [73, 75, 76], the production of such solitons in the kagome photonic lattice is still an open problem. To the best of our knowledge, nonlinear manipulation of the valley

Hall edge states in the kagome photonic lattice is not reported yet. This is accomplished in this work.

We believe that research on topological solitons in kagome (or any other) lattice is meaningful and significant, because it not only deepens the understanding of valley Hall effect and provides a new method for manipulating light field in a photonic crystal, but also enlightens future ideas that might help the development of on-chip optical functional devices, *e.g.*, the valley Hall lasing in the kagome photonic lattice.

2. CONFIGURATION AND BAND STRUCTURE

The propagation dynamics of the valley Hall edge state along the longitudinal z axis of the waveguide array with focusing cubic nonlinearity can be described by the dimensionless nonlinear Schrödinger-like paraxial wave equation,

$$i\frac{\partial\psi}{\partial z} = -\frac{1}{2}\left(\frac{\partial^2}{\partial x^2} + \frac{\partial^2}{\partial y^2}\right)\psi - \mathcal{R}(x,y)\psi - |\psi|^2\psi, \tag{1}$$

where ψ is the field amplitude, $x = X/r_0$ and $y = Y/r_0$ are the normalized transverse coordinates, and $z = Z/(\kappa r_0^2)$ is the normalized propagation distance. Here, r_0 is the transverse scale, $\kappa = 2n\pi/\lambda$ the wavenumber, λ the wavelength, and n the ambient refractive index. The potential function $\mathcal{R}$ stands for the waveguide array that is arranged within a kagome landscape without any modulation along the longitudinal coordinate. The profiles of individual waveguides in the array are described by Gaussian functions of width d:

$$\mathcal{R}(x,y) = p\sum_{m,n}\exp\left[-\frac{(x-x_{m,n})^2 + (y-y_{m,n})^2}{d^2}\right], \tag{2}$$

where p stands for the depth of waveguides in two sublattices, and $(x_{m,n}, y_{m,n})$ are the coordinates of the nodes in the kagome grid. We consider a configuration that is periodic along the x axis and is limited along the y axis, with outer boundaries located far away from the domain wall, so that $\mathcal{R}(x,y) = \mathcal{R}(x+L,y)$ with $L = 2a$ and a being the array constant, as shown in Fig. 1(a). Clearly, the distance between two nearest-neighbored sites in Fig. 1(a) is also a. Representative parameter values for these quantities are $a = 1.7$, $d = 0.5$ (in units of r_0), and $p = 12$. By inserting the ansatz $\psi(x,y,z) = u(x,y)\exp(ik_x x)\exp(ibz)$ into Eq. (1) and without considering the nonlinear term, one obtains the linear eigenvalue problem

$$bu = \frac{1}{2}\left(\frac{\partial^2}{\partial x^2} + \frac{\partial^2}{\partial y^2} + 2ik_x\frac{\partial}{\partial x} - k_x^2\right)u + \mathcal{R}u, \tag{3}$$

where $u(x,y) = u(x+L,y)$ is the periodic Bloch wave function, $k_x \in [-\mathrm{K}_x/2, \mathrm{K}_x/2)$ is the Bloch momentum in the first Brillouin zone with $\mathrm{K}_x = 2\pi/L$, and b is the prop-

agation constant of the linear mode that is a function of k_x. Based on the plane-wave expansion method, the band structure corresponding to the configuration in Fig. 1(a) is easily obtained, as displayed on the right-hand-side of the configuration, which is projected onto the (k_x, b) plane - it has three bands and there are Dirac points between the top two bands.

The configuration can be experimentally obtained by using the femtosecond laser writing technique in fused silica [3, 8, 10, 11, 90, 93], and the dimensionless parameters described above can be switched to dimensional ones with real physical meaning. Provided the laser radiation at the wavelength of $\lambda = 800$ nm is used and the characteristic transverse scale is set to $r_0 = 10$ μm that corresponds to dimensionless coordinates $x, y = 1$, the array constant is 17 μm, the waveguide width is 5 μm, and the refractive index modulation depth is $\sim 1.07 \times 10^{-4}$ per unit depth.

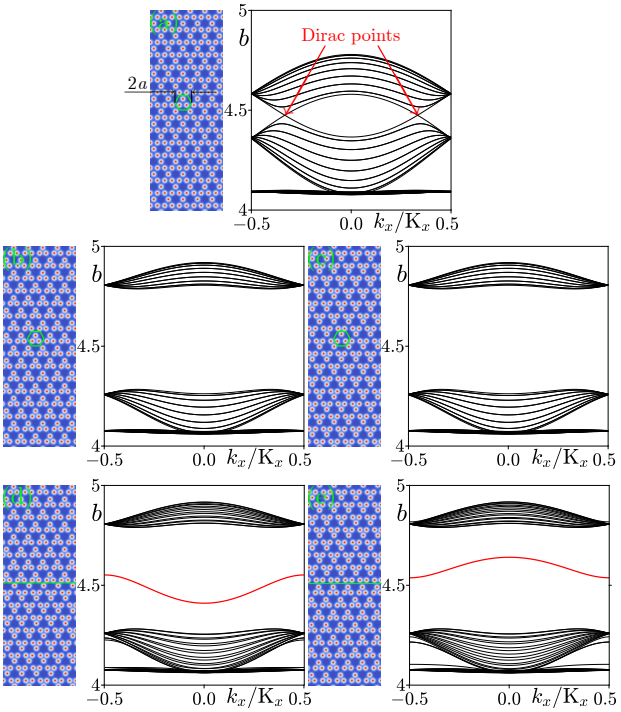

Fig. 1 – (Color online) (a) Kagome photonic lattice and its corresponding band struture projected on the (k_x, b) plane, which possesses two Dirac points. The green hexagon shows the unit cell that has three sites. (b) Setup is as in (a), but for the squeezed kagome lattice. In the band structure, Dirac points disappear and the band gap appears. (c) Setup is as in (b), but for the expanded kagome lattice. (d) Composite kagome lattice with squeezed (top) and expanded (bottom) kagome lattices, with the interface indicated by the green line. There is an edge state in the band structure that is indicated by the red curve. (e) Setup is as in (d), but with expanded (top) and squeezed (bottom) kagome lattices. Parameters: $a = 1.7$, $d = 0.5$, $p = 12$, and $\delta = 0.2$.

For enabling the valley Hall effect in kagome lattice, one has to squeeze/expand the distance among three sites in the unit cell [91, 92] and at the same time keep the distance between two neighboring unit cells unchanged. After this operation, the rotation symmetry of the configuration changes from C_6 to C_3. To conveniently evaluate the shrinkage and expansion within the unit cell, we introduce a positive quantity δ. Thus, the distance among three sites in one unit cell is changed to $\alpha = a - \delta$ for the squeezed kagome lattice and to $\alpha = a + \delta$ for the expanded kagome lattice. The squeezed and expanded kagome lattices with $\delta = 0.2$ are shown in Figs. 1(b) and 1(c), respectively. From the corresponding band structures, one finds that the Dirac points between top two bands are replaced by a big band gap. Even though the band structures in Figs. 1(b) and 1(c) look the same, the corresponding Berry curvatures are opposite [91, 92], which is crucial for establishing a domain wall between the squeezed and expanded kagome lattice arrays, and realizing the valley Hall edge state. In Figs. 1(d) and 1(e), we show the composite kagome lattice, by combining the squeezed lattice and the expanded lattice with the interface highlighted by a green line. The difference between the two configurations is that the top lattice is squeezed in Fig. 1(d) while the bottom lattice is squeezed in Fig. 1(e). One finds that both cases can support valley Hall edge states in the band gap, as indicated by red curves in the band structures.

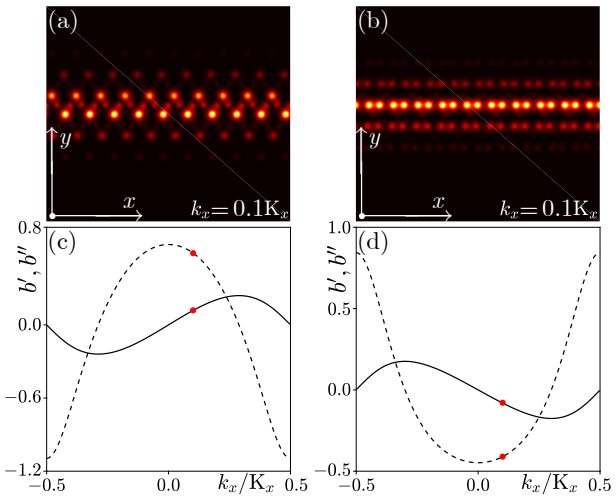

Fig. 2 – (a) Linear valley Hall edge state at $k_x = 0.1\mathrm{K}_x$ in Fig. 1(d). (b) Linear valley Hall edge state at $k_x = 0.1\mathrm{K}_x$ in Fig. 1(e). (c) First-order $b' = db/dk_x$ and second-order $b'' = d^2b/dk_x^2$ derivatives of the valley Hall edge state in Fig. 1(d), as shown by the solid and dashed curves, respectively. (d) Same as in (c), but for the edge state in Fig. 1(e).

We present in Fig. 2 the valley Hall edge state at $k_x = 0.1\mathrm{K}_x$ for both cases in

Figs. 1(d) and 1(e), displayed in Figs. 2(a) and 2(b), respectively. One finds that the energy is indeed mostly localized along the domain wall. To exhibit more intricate properties of these edge states, we explore their first-order $b' = db/dk_x$ and second-order $b'' = d^2b/dk_x^2$ derivatives, as shown in Figs. 2(c) and 2(d), which correspond to valley Hall edge states in Figs. 1(d) and 1(e). The red dots elucidate the Bloch momentum $k_x = 0.1\mathrm{K}_x$. As is well known, b' estimates the velocity of the edge state ($v = -b'$) while b'' is responsible for its dispersion. According to the condition for constructing bright and dark solitons, the valley Hall edge state with the negative second-order derivative supports bright valley Hall edge solitons and that with the positive second-order derivative supports dark valley Hall edge solitons. Hence, one expects a dark valley Hall edge soliton based on the state in Fig. 2(c) and a bright valley Hall edge soliton based on the state in Fig. 2(d).

3. VALLEY HALL EDGE SOLITONS

To construct bright valley Hall edge solitons, one firstly establishes the nonlinear valley Hall edge state, and then seeks for the precursor of the valley Hall edge soliton, due to the splitting spot of the valley Hall edge state, that will grow thanks to the incipient modulational instability [48, 73, 75]. However, this method is not appropriate for the dark valley Hall edge soliton, which displays a notch on the homogeneous background. Therefore, we adopted the method developed in Refs. [69, 72], according to which the soliton can be prepared by superimposing the envelopes of the linear valley Hall edge state. The envelope equation corresponding to Eq. (1) can be written as

$$i\frac{\partial A}{\partial z} = \frac{\beta''}{2}\frac{\partial^2 A}{\partial X^2} - \chi|A|^2 A, \tag{4}$$

where A is the slowly-varying envelope, $\chi = \int_{-\infty}^{+\infty} dy \int_0^L |\phi|^4 dx$ is the nonlinearity coefficient, and $X = x + b'z$. The soliton solution can be written in the form $\psi(x, y, z) = A(X, z)\phi(x, y)\exp(ibz)$, in which $\phi(x, y)\exp(ibz)$ is the linear Bloch state. Bright solitons exist in the region $b'' < 0$, while dark solitons exist in the region $b'' > 0$. Numerically, Eq. (4) can be solved by using Newton's method in the form $A(X, z) = w(X)\exp(ib_{\mathrm{nl}}z)$, where b_{nl} is the nonlinearity-induced phase shift, which should be sufficiently small to make sure that the profile $w(X)$ is broad and fulfills the slowly-varying requirement. Equation (4) is the well-known nonlinear Schrödinger equation with third-order nonlinearity (*i.e.*, the Kerr nonlinearity), and it possesses various solutions. We are interested in the soliton solutions that can be written as

$$A(x, z) = \sqrt{2\frac{b_{\mathrm{nl}}}{\chi}}\,\mathrm{sech}\left(\sqrt{-2\frac{b_{\mathrm{nl}}}{b''}}\left(x + b'z\right)\right)\exp\left(-ib_{\mathrm{nl}}z\right) \tag{5}$$

for bright solitons, and

$$A(x,z)=\sqrt{\frac{b_{\mathrm{nl}}}{\chi}}\tanh\left(\sqrt{\frac{b_{\mathrm{nl}}}{b''}}\left(x+b'z\right)\right)\exp\left(-ib_{\mathrm{nl}}z\right) \tag{6}$$

for dark solitons.

3.1. BRIGHT VALLEY HALL EDGE SOLITONS

By superimposing the envelope in Eq. (5) to the corresponding linear valley Hall edge state shown in Fig. 2(b), we obtain the bright valley Hall edge soliton with $b_{\mathrm{nl}}=0.003$ at $k_x=0.1\mathrm{K}_x$, as shown in Fig. 3(a) at distance $z=0$. Since the first-order derivative of the linear valley Hall edge state is $b'=-0.0805$, the bright valley Hall edge state moves along the positive x direction during propagation, with a speed of $v=0.0805$, as the soliton bifurcates from the linear valley Hall edge state. The movement can be seen from the selective profiles at certain distances, shown in each panel. The beam can maintain its profile unchanged even after experiencing an extremely long propagation distance, *e.g.*, $z=10000$. As an illustration, we record the peak amplitude $a_{\mathrm{nlin}}=\max\{|\psi|\}$ during propagation, shown by the black curve in Fig. 3(c). One finds that the peak amplitude indeed does not decay.

If the nonlinearity is lifted during propagation, the diffraction will result in the broadening of the beam. To demonstrate the significance of nonlinearity, we display the profile of the beam at $z=2000$ upon linear propagation in Fig. 3(b) - the domain wall is almost filled with the beam because of the diffractive broadening, which is sharply different from the nonlinear propagation in Fig. 3(a). The broadening of the beam must be accompanied by decreasing peak amplitude, and this phenomenon is demonstrated by the red curve in Fig. 3(c), which is the peak amplitude of the beam during linear propagation a_{lin}. Clearly, the formation of the bright valley Hall edge soliton is due to the balance between the nonlinearity and the diffraction.

3.2. DARK VALLEY HALL EDGE SOLITONS

To construct the dark valley Hall edge soliton, we superimpose the linear valley Hall edge state in Fig. 2(a) with the envelope given in Eq. (6). Since there is a π-phase shift across the notch, we investigate the propagation dynamics of two dark valley Hall edge solitons with a large separation. This operation is necessary, and the reason is two-fold. Firstly, we use the split-step Fourier method to do the propagation, which will connect the left-end (viz. $\min\{x\}$) and right-end (viz. $\max\{x\}$) of the window to make a loop that demands $\psi|_{\min\{x\}}=\psi|_{\max\{x\}}$. Secondly, there must be interaction between solitons [76] if they are close to each other, hence large separation will prevent such an interaction. In Fig. 4(a), the constructed dark valley

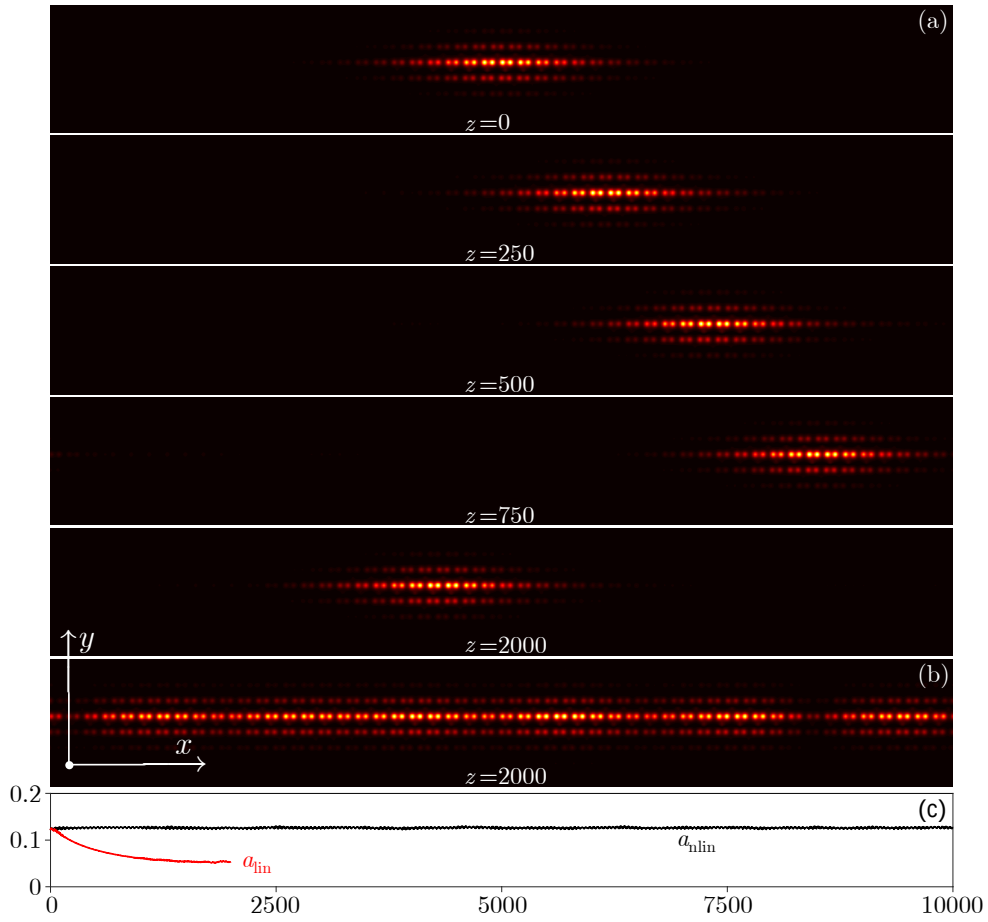

Fig. 3 – (Color online) (a) Profiles of the bright valley Hall edge soliton with $k_x = 0.1\mathrm{K}_x$ at selected distances during propagation. (b) Profile of the same input as in (a), but for linear propagation. (c) Peak amplitude of the beam during propagation. Black curve is for nonlinear propagation, while the red curve is for linear propagation. All panels are shown in the window $-85 \leq x \leq 85$ and $-12 \leq y \leq 12$. For the envelope, we use $b_{\rm nl} = 0.003$, $b' = -0.0805$, $b'' = -0.4111$, and other parameters are the same as those adopted in Fig. 1.

Hall edge solitons (with $z = 0$ at the bottom of the panel) localize at $x = \pm 80$ with $\max\{x\} = 136$, so the separation of the two dark valley Hall edge solitons is 160 or 112, which is sufficiently large to avoid the interaction between solitons.

Since $b' = 0.1175$, the dark valley Hall edge soliton moves along the negative x direction with a speed $v = -0.1175$ during propagation, as exhibited in the selected profiles in Fig. 4. One also finds that the launched beam maintains its shape without decaying during propagation, which elucidates the validity of the existence of the dark valley Hall edge soliton. Similar to the bright case, we also record the linear

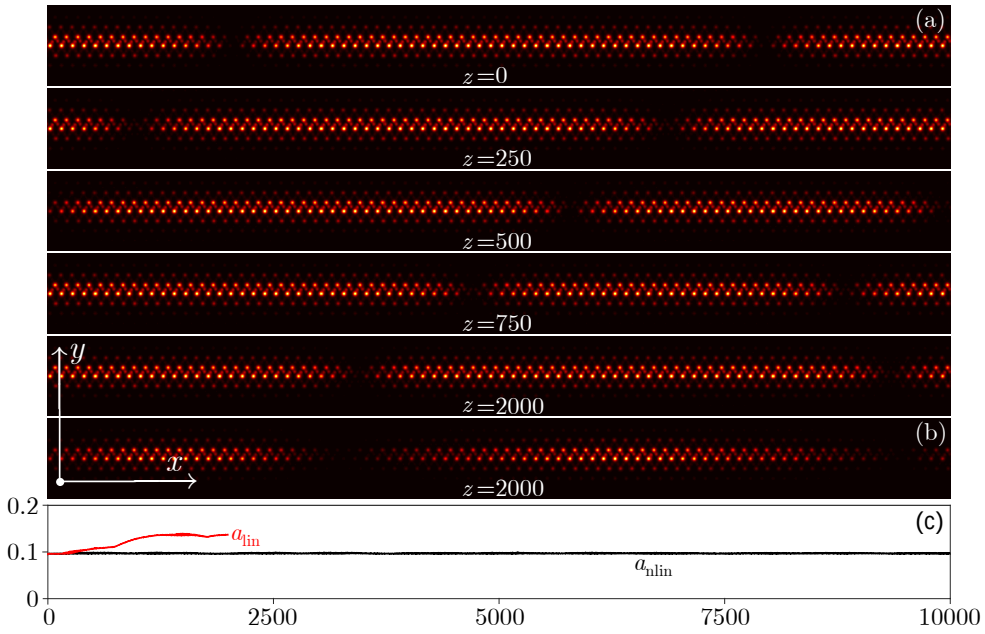

Fig. 4 – (Color online) Same as Fig. 3 but for the dark valley Hall edge soliton with $b_{\rm nl} = 0.003$, $b' = 0.1175$ and $b'' = 0.5898$. All panels are shown in the window $-136 \leq x \leq 136$ and $-12 \leq y \leq 12$.

propagation of the beam in Fig. 4(a) with $z = 0$, and the profile at $z = 2000$ is displayed in Fig. 4(b). In comparison with the profile at $z = 2000$ in Fig. 4(a), the notch width in Fig. 4(b) is much wider, because of the diffractive broadening. Different from the bright case, where one can record the peak amplitude during propagation, there is no peak amplitude for the dark valley Hall edge soliton, except the background peak amplitude. In Fig. 4(c), we show the background amplitude peak for both nonlinear propagation $a_{\rm nlin}$ and linear propagation $a_{\rm lin}$, as indicated by the black and red curves, respectively. One finds that the background amplitude peak $a_{\rm nlin}$ does not change over a long propagation distance, which demonstrates the stability of the dark valley Hall edge soliton, whereas the background amplitude peak $a_{\rm lin}$ increases upon linear propagation. The profile of the beam in Fig. 4(b) as well as the background amplitude peak in Fig. 4(c) affirms the decisive role of nonlinearity in the formation of dark valley Hall edge solitons.

3.3. TOPOLOGICAL PROTECTION OF VALLEY HALL EDGE SOLITONS

In the above text, we have demonstrated the existence and propagation dynamics of both bright and dark valley Hall edge solitons in the kagome lattice waveguide arrays. In this subsection, we confirm the topological protection of these valley Hall

edge solitons, by exhibiting their capability of circumventing sharp corners. Even though the squeezed and expanded kagome lattices lost their C_6 rotation symmetry, they still possess the C_3 rotation symmetry, so that establishing a domain wall with 60° or 120° corners is feasible. In Fig. 5(a), we display a composite kagome lattice with a plough-shaped domain wall, as indicated by the green line. The angle at the corner is 60°.

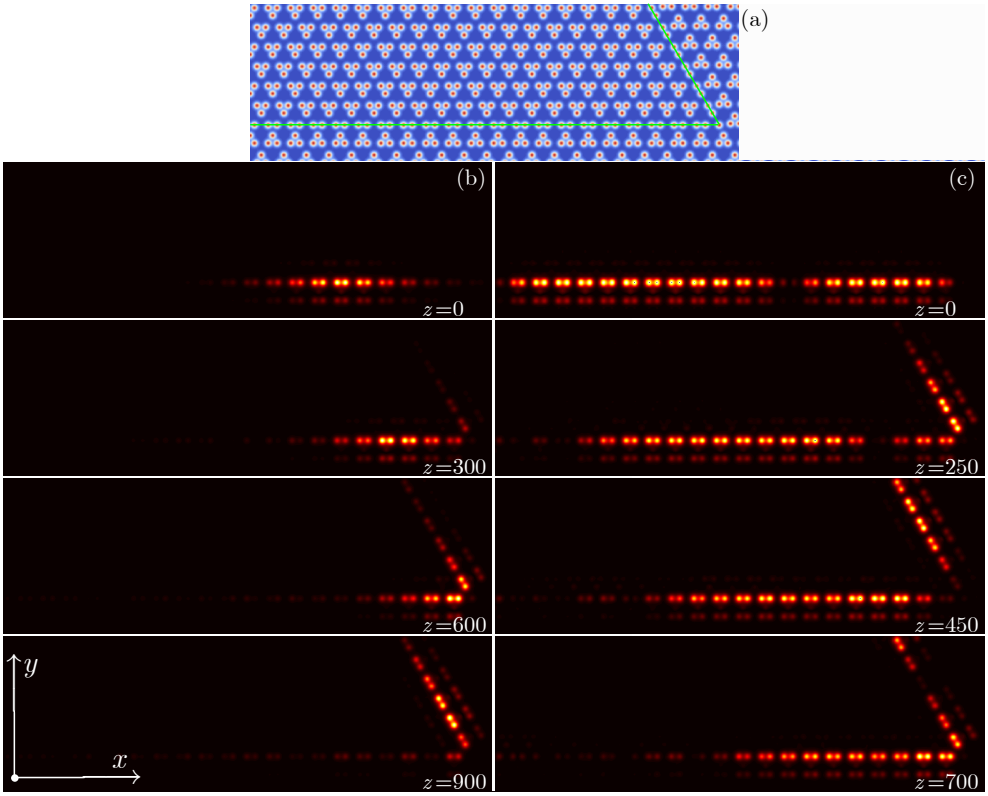

Fig. 5 – (a) Navigating kagome lattice with a plough-shaped domain wall as indicated by the green line. (b) Propagation of the bright valley Hall edge soliton along the domain wall at selective distances. All panels are shown in the window $-72 \leq x \leq 72$ and $-5 \leq y \leq 20$. Other parameters: $a = 1.8$, $\delta = 0.4$, $d = 0.5$, $b' = -0.0336$, $b'' = -0.1718$, $b_{\rm nl} = 0.003$, and $k_x = 0.1\mathrm{K}_x$. (c) Same as in (b) but for the dark valley Hall edge state with $b' = -0.0666$, $b'' = 0.0031$, $b_{\rm nl} = 0.0001$ and $k_x = 0.265\mathrm{K}_x$.

We first launch a bright valley Hall edge soliton into the horizontal edge of the domain wall, as shown in the panel with $z = 0$ in Fig. 5(b). Since the velocity is along the positive x direction, the valley Hall edge soliton will encounter the corner during propagation (see the panel with the distance $z = 300$). When it propagates to $z = 600$, nearly half of the energy transfers to sloped edge of the domain wall.

The bright valley Hall edge soliton almost moves away from the sloped edge after a propagation distance of $z = 900$, with a small residual on the horizontal edge. This phenomenon demonstrates that the bright valley Hall edge state can circumvent the sharp corner and is topologically protected. The right column in Fig. 5 displays the case of the dark valley edge soliton.

As shown in Fig. 1(d) and Fig. 1(e), the second-order derivative of the edge state can be positive or negative, which depends on the value of Bloch momentum. For checking the topological protection of dark valley Hall edge state, we still use the same configuration as in Fig. 5(a), but we choose $k_x = 0.265\mathrm{K}_x$. Frankly, according to the definition of dark soliton, the homogeneous background should fill both the horizontal edge and the sloped edge of the domain wall. However, this is difficult to reach. As a compromise, we can only prepare a quasi-soliton as shown in Fig. 5(c) at $z = 0$, which is along the horizontal edge of the domain wall. We agree that the quasi-soliton will spread during propagation, but still we can record the behavior of the notch, which moves along the positive x direction (see the profile at $z = 250$). When the beam reaches $z = 450$, the notch is crossing the corner without showing much of reflection or radiation. The notch completely transfers to the sloped edge of the domain wall finally, and the profile demonstrating this phenomenon is also shown in Fig. 5(c), at $z = 700$. In this manner, we have exhibited the topological protection of valley Hall edge solitons.

4. CONCLUSION

Summarizing, we have demonstrated the existence and dynamics of valley Hall edge solitons in the kagome lattice, for the first time. By combining the squeezed and expanded kagome lattices, a domain wall (*i.e.*, the interface) is established between them that supports valley Hall edge soliton states. According to the dispersive properties of the edge state, we successfully constructed both bright and dark valley Hall edge solitons by superimposing envelopes onto their corresponding linear valley Hall edge states. The valley Hall edge solitons in the kagome lattice propagate stably and are topologically protected, because they can circumvent sharp corners set in the domain wall. These results not only help to better understand the valley Hall effect, but also display the potential for applications in fabricating compact on-chip optical functional devices on-demand.

Acknowledgements. This work is supported by the National Natural Science Foundation of China (Nos. 12074308, U1537210) and the Fundamental Research Funds for the Central Universities (No. xzy012019038). Work in Qatar is supported by the NPRP-11S-1126-170033 project from the Qatar National Research Fund (a member of the Qatar Foundation).

REFERENCES

1. M. Z. Hasan, C. L. Kane, Rev. Mod. Phys. **82**, 3045–3067 (2010).
2. X.-L. Qi, S.-C. Zhang, Rev. Mod. Phys. **83**, 1057–1110 (2011).
3. M. C. Rechtsman, J. M. Zeuner, Y. Plotnik, Y. Lumer, D. Podolsky, F. Dreisow, S. Nolte, M. Segev, A. Szameit, Nature **496**, 196–200 (2013).
4. F. D. M. Haldane, S. Raghu, Phys. Rev. Lett. **100**, 013904 (2008).
5. Z. Wang, Y. Chong, J. D. Joannopoulos, M. Soljačić, Nature **461**, 772–775 (2009).
6. N. H. Lindner, G. Refael, V. Galitski, Nat. Phys. **7**, 490–495 (2011).
7. M. Hafezi, E. A. Demler, M. D. Lukin, J. M. Taylor, Nat. Phys. **7**, 907–912 (2011).
8. S. Stützer, Y. Plotnik, Y. Lumer, P. Titum, N. H. Lindner, M. Segev, M. C. Rechtsman, A. Szameit, Nature **560**, 461–465 (2018).
9. Y. Yang, Z. Gao, H. Xue, L. Zhang, M. He, Z. Yang, R. Singh, Y. Chong, B. Zhang, H. Chen, Nature **565**, 622–626 (2019).
10. S. Mukherjee, M. C. Rechtsman, Science **368**, 856–859 (2020).
11. L. J. Maczewsky, M. Heinrich, M. Kremer, S. K. Ivanov, M. Ehrhardt *et al.*, Science **370**, 701–704 (2020).
12. Z. Yang, E. Lustig, Y. Lumer, M. Segev, Light Sci. Appl. **9**, 128 (2020).
13. Z. Yang, F. Gao, X. Shi, X. Lin, Z. Gao, Y. Chong, B. Zhang, Phys. Rev. Lett. **114**, 114301 (2015).
14. Y.-G. Peng, C.-Z. Qin, D.-G. Zhao, Y.-X. Shen, X.-Y. Xu, M. Bao, H. Jia, X.-F. Zhu, Nat. Commun. **7**, 13368 (2016).
15. C. He, X. Ni, H. Ge, X.-C. Sun, Y.-B. Chen, M.-H. Lu, X.-P. Liu, Y.-F. Chen, Nat. Phys. **12**, 1124–1129 (2016).
16. J. Lu, C. Qiu, L. Ye, X. Fan, M. Ke, F. Zhang, Z. Liu, Nat. Phys. **13**, 369–374 (2017).
17. X. Zhang, M. Xiao, Y. Cheng, M.-H. Lu, J. Christensen, Commun. Phys. **1**, 97 (2018).
18. G. Ma, M. Xiao, C. T. Chan, Nat. Rev. Phys. **1**, 281–294 (2019).
19. R. Süsstrunk, S. D. Huber, Science **349**, 47–50 (2015).
20. S. D. Huber, Nat. Phys. **12**, 621–623 (2016).
21. N. Goldman, J. Dalibard, A. Dauphin, F. Gerbier, M. Lewenstein, P. Zoller, I. B. Spielman, Proc. Natl. Acad. Sci. **110**, 6736–6741 (2013).
22. G. Jotzu, M. Messer, R. Desbuquois, M. Lebrat, T. Uehlinger, D. Greif, T. Esslinger, Nature **515**, 237–240 (2014).
23. A. V. Nalitov, D. D. Solnyshkov, G. Malpuech, Phys. Rev. Lett. **114**, 116401 (2015).
24. P. St-Jean, V. Goblot, E. Galopin, A. Lemaître, T. Ozawa, L. Le Gratiet, I. Sagnes, J. Bloch, A. Amo, Nat. Photon. **11**, 651–656 (2017).
25. S. Klembt, T. H. Harder, O. A. Egorov, K. Winkler, R. Ge *et al.*, Nature **562**, 552–556 (2018).
26. V. V. Albert, L. I. Glazman, L. Jiang, Phys. Rev. Lett. **114**, 173902 (2015).
27. Y. Hadad, J. C. Soric, A. B. Khanikaev, A. Alù, Nat. Electron. **1**, 178–182 (2018).
28. S. Imhof, C. Berger, F. Bayer, J. Brehm, L. W. Molenkamp *et al.*, Nature Physics **14**, 925–929 (2018).
29. N. A. Olekhno, E. I. Kretov, A. A. Stepanenko, P. A. Ivanova, V. V. Yaroshenko, E. M. Puhtina, D. S. Filonov, B. Cappello, L. Matekovits, M. A. Gorlach, Nat. Commun. **11**, 1436 (2020).
30. T. Helbig, T. Hofmann, S. Imhof, M. Abdelghany, T. Kiessling, L. W. Molenkamp, C. H. Lee, A. Szameit, M. Greiter, R. Thomale, Nat. Phys. **16**, 747–750 (2020).
31. R. Li, B. Lv, H. Tao, J. Shi, Y. Chong, B. Zhang, H. Chen, National Sci. Rev. **8**, nwaa192 (2020).
32. L. Lu, J. D. Joannopoulos, M. Soljačić, Nat. Photon. **8**, 821–829 (2014).

33. T. Ozawa, H. M. Price, A. Amo, N. Goldman, M. Hafezi *et al.*, Rev. Mod. Phys. **91**, 015006 (2019).
34. M. Kim, Z. Jacob, J. Rho, Light Sci. Appl. **9**, 130 (2020).
35. D. Smirnova, D. Leykam, Y. Chong, Y. Kivshar, Appl. Phys. Rev. **7**, 021306 (2020).
36. Y. Ota, K. Takata, T. Ozawa, A. Amo, Z. Jia, B. Kante, M. Notomi, Y. Arakawa, S. Iwamoto, Nanophoton. **9**, 547–567 (2020).
37. D. Leykam, L. Yuan, Nanophoton. **9**, 4473–4487 (2020).
38. M. Segev, M. A. Bandres, Nanophoton. **10**, 425–434 (2021).
39. M. Parto, Y. G. N. Liu, B. Bahari, M. Khajavikhan, D. N. Christodoulides, Nanophoton. **10**, 403–423 (2021).
40. H. Wang, S. K. Gupta, B. Xie, M. Lu, Front. Optoelectron. **13**, 50–72 (2020).
41. H. Liu, B. Xie, H. Cheng, J. Tian, S. Chen, Chin. Opt. Lett. **19**, 052602 (2021).
42. H. Wang, X. Zhang, J. Hua, D. Lei, M. Lu, Y. Chen, J. Opt. **23**, 123001 (2021).
43. Q. Yan, X. Hu, Y. Fu, C. Lu, C. Fan, Q. Liu, X. Feng, Q. Sun, Q. Gong, Adv. Opt. Mater. **9**, 2001739 (2021).
44. Y. V. Kartashov, D. V. Skryabin, Phys. Rev. Lett. **119**, 253904 (2017).
45. W. Zhang, X. Chen, Y. V. Kartashov, D. V. Skryabin, F. Ye, Laser Photon. Rev. **13**, 1900198 (2019).
46. Y. Q. Zhang, Y. V. Kartashov, A. Ferrando, Phys. Rev. A **99**, 053836 (2019).
47. Y. Lumer, M. C. Rechtsman, Y. Plotnik, M. Segev, Phys. Rev. A **94**, 021801 (2016).
48. Y. V. Kartashov, D. V. Skryabin, Optica **3**, 1228–1236 (2016).
49. G. Harari, M. A. Bandres, Y. Lumer, M. C. Rechtsman, Y. D. Chong, M. Khajavikhan, D. N. Christodoulides, M. Segev, Science **359**, eaar4003 (2018).
50. M. A. Bandres, S. Wittek, G. Harari, M. Parto, J. Ren, M. Segev, D. N. Christodoulides, M. Khajavikhan, Science **359**, eaar4005 (2018).
51. A. Dikopoltsev, T. H. Harder, E. Lustig, O. A. Egorov, J. Beierlein *et al.*, Science **373**, 1514–1517 (2021).
52. B. Bahari, A. Ndao, F. Vallini, A. El Amili, Y. Fainman, B. Kanté, Science **358**, 636–640 (2017).
53. Y. V. Kartashov, D. V. Skryabin, Phys. Rev. Lett. **122**, 083902 (2019).
54. Y. Zeng, U. Chattopadhyay, B. Zhu, B. Qiang, J. Li *et al.*, Nature **578**, 246–250 (2020).
55. H. Zhong, Y. D. Li, D. H. Song, Y. V. Kartashov, Y. Q. Zhang, Y. P. Zhang, Z. Chen, Laser Photon. Rev. **14**, 2000001 (2020).
56. Y. Gong, S. Wong, A. J. Bennett, D. L. Huffaker, S. S. Oh, ACS Photon. **7**, 2089–2097 (2020).
57. X. Liu, L. Zhao, D. Zhang, S. Gao, Opt. Express **30**, 4965–4977 (2022).
58. Y. V. Kartashov, G. E. Astrakharchik, B. A. Malomed, L. Torner, Nat. Rev. Phys. **1**, 185–197 (2019).
59. B. A. Malomed, D. Mihalache, Rom. J. Phys. **64**, 106 (2019).
60. D. Mihalache, Rom. Rep. Phys. **73**, 403 (2021).
61. Y. Lumer, Y. Plotnik, M. C. Rechtsman, M. Segev, Phys. Rev. Lett. **111**, 243905 (2013).
62. O. Bleu, G. Malpuech, D. D. Solnyshkov, Nat. Commun. **9**, 3991 (2018).
63. D. Leykam, Y. D. Chong, Phys. Rev. Lett. **117**, 143901 (2016).
64. M. J. Ablowitz, J. T. Cole, Phys. Rev. A **96**, 043868 (2017).
65. D. R. Gulevich, D. Yudin, D. V. Skryabin, I. V. Iorsh, I. A. Shelykh, Sci. Rep. **7**, 1780 (2017).
66. C. Li, F. Ye, X. Chen, Y. V. Kartashov, A. Ferrando, L. Torner, D. V. Skryabin, Phys. Rev. B **97**, 081103 (2018).
67. D. A. Smirnova, L. A. Smirnov, D. Leykam, Y. S. Kivshar, Laser Photon. Rev. **13**, 1900223 (2019).
68. W. Zhang, X. Chen, Y. V. Kartashov, V. V. Konotop, F. Ye, Phys. Rev. Lett. **123**, 254103 (2019).

69. S. K. Ivanov, Y. V. Kartashov, A. Szameit, L. Torner, V. V. Konotop, ACS Photon. **7**, 735–745 (2020).
70. S. K. Ivanov, Y. V. Kartashov, L. J. Maczewsky, A. Szameit, V. V. Konotop, Opt. Lett. **45**, 1459–1462 (2020).
71. S. K. Ivanov, Y. V. Kartashov, L. J. Maczewsky, A. Szameit, V. V. Konotop, Opt. Lett. **45**, 2271–2274 (2020).
72. S. K. Ivanov, Y. V. Kartashov, M. Heinrich, A. Szameit, L. Torner, V. V. Konotop, Phys. Rev. A **103**, 053507 (2021).
73. H. Zhong, S. Xia, Y. Zhang, Y. Li, D. Song, C. Liu, Z. Chen, Adv. Photon. **3**, 056001 (2021).
74. D. A. Smirnova, L. A. Smirnov, E. O. Smolina, D. G. Angelakis, D. Leykam, Phys. Rev. Research **3**, 043027 (2021).
75. Q. Tang, B. Ren, V. O. Kompanets, Y. V. Kartashov, Y. Li, Y. Zhang, Opt. Express **29**, 39755–39765 (2021).
76. B. Ren, H. Wang, V. O. Kompanets, Y. V. Kartashov, Y. Li, Y. Zhang, Nanophoton. **10**, 3559–3566 (2021).
77. M. Guo, S. Xia, N. Wang, D. Song, Z. Chen, J. Yang, Opt. Lett. **45**, 6466–6469 (2020).
78. S. Xia, D. Jukić, N. Wang, D. Smirnova, L. Smirnov *et al.*, Light Sci. Appl. **9**, 147 (2020).
79. F. Zangeneh-Nejad, R. Fleury, Phys. Rev. Lett. **123**, 053902 (2019).
80. J.-W. Liu, F.-L. Shi, X.-T. He, G.-J. Tang, W.-J. Chen, X.-D. Chen, J.-W. Dong, Adv. Phys. X **6**, 1905546 (2021).
81. R. A. Vicencio, C. Cantillano, L. Morales-Inostroza, B. Real, C. Mejía-Cortés, S. Weimann, A. Szameit, M. I. Molina, Phys. Rev. Lett. **114**, 245503 (2015).
82. S. Mukherjee, A. Spracklen, D. Choudhury, N. Goldman, P. Öhberg, E. Andersson, R. R. Thomson, Phys. Rev. Lett. **114**, 245504 (2015).
83. H. Zhong, R. Wang, F. Ye, J. Zhang, L. Zhang, Y. Zhang, M. R. Belić, Y. Zhang, Results Phys. **12**, 996–1001 (2019).
84. H. Xue, Y. Yang, F. Gao, Y. Chong, B. Zhang, Nat. Mater. **18**, 108–112 (2019).
85. X. Ni, M. Weiner, A. Al., A. B. Khanikaev, Nat. Mater. **18**, 113–120 (2019).
86. A. El Hassan, F. K. Kunst, A. Moritz, G. Andler, E. J. Bergholtz, M. Bourennane, Nat. Photon. **13**, 697–700 (2019).
87. M. Li, D. Zhirihin, M. Gorlach, X. Ni, D. Filonov, A. Slobozhanyuk, A. Alú, A. B. Khanikaev, Nat. Photon. **14**, 89–94 (2020).
88. Y. Zhang, Y. V. Kartashov, L. Torner, Y. Li, A. Ferrando, Opt. Lett. **45**, 4710–4713 (2020).
89. H. Zhong, Y. V. Kartashov, A. Szameit, Y. Li, C. Liu, Y. Zhang, APL Photon. **6**, 040802 (2021).
90. M. S. Kirsch, Y. Zhang, M. Kremer, L. J. Maczewsky, S. K. Ivanov, Y. V. Kartashov, L. Torner, D. Bauer, A. Szameit, M. Heinrich, Nat. Phys. **17**, 995–1000 (2021).
91. N. Lera, D. Torrent, P. San-Jose, J. Christensen, J. V. Alvarez, Phys. Rev. B **99**, 134102 (2019).
92. S. Wong, M. Saba, O. Hess, S. S. Oh, Phys. Rev. Research **2**, 012011 (2020).
93. D. Tan, Z. Wang, B. Xu, J. Qiu, Adv. Photon. **3**, 024002 (2021).